Supporting Information: Lattice Strain Measurement of Core@Shell Electrocatalysts with 4D Scanning Transmission Electron Microscopy Nanobeam Electron Diffraction

Debangshu Mukherjee,*,† Jocelyn T.L. Gamler,‡ Sara E. Skrabalak,‡ and Raymond R. Unocic*,†

†*Center for Nanophase Materials Sciences, Oak Ridge National Laboratory, Oak Ridge, Tennessee 37831, United States*

‡*Department of Chemistry, Indiana University – Bloomington, Bloomington, Indiana 47405, United States*

E-mail: mukherjeed@ornl.gov; unocicrr@ornl.gov

1 Effects of scan distortions on strain

ADF-STEM datasets were collected using two orthogonal scan directions, shown as Figure S1(a) and Figure S2(a). A flyback scanning procedure was used for both the scanning images, where the electron scans along a direction (also referred to as the *fast scan direction*), and after completion of each scan line returns back to the initial scan position, shifts down by a single pixel spacing and then starts scanning the subsequent line. As could be ascertained, thus the velocity of beam movement along the direction orthogonal to the fast scan direction is almost three orders of magnitude slower.

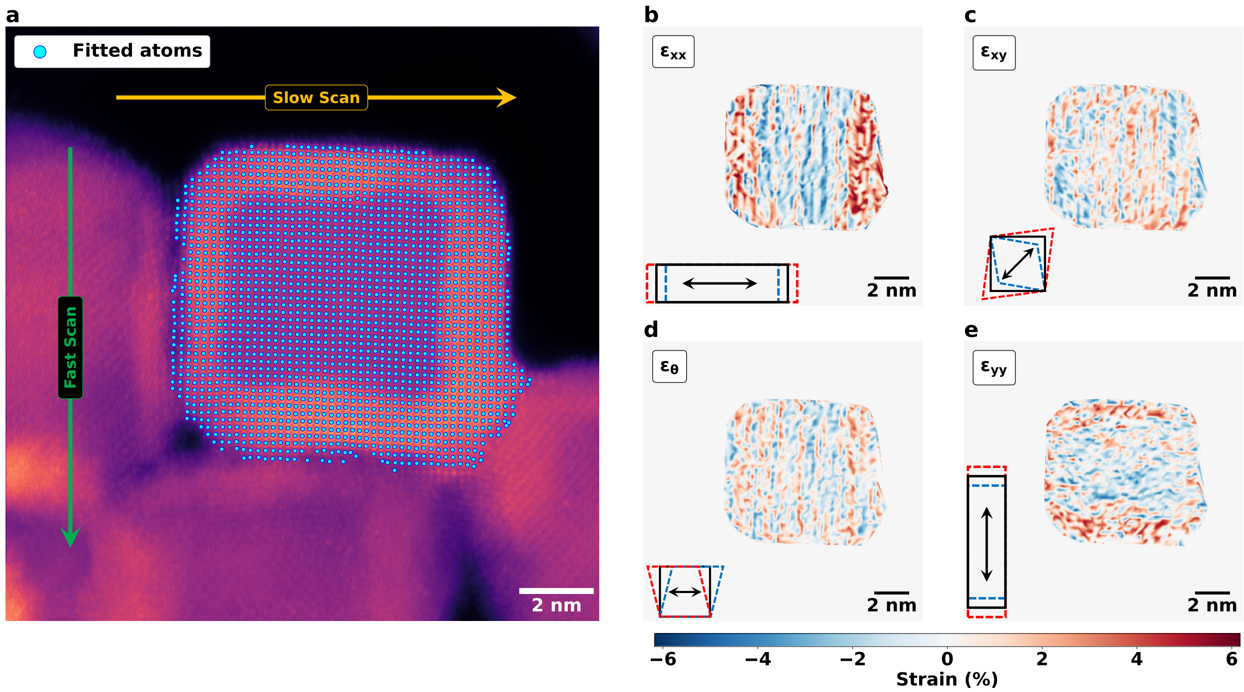

Figure S1: **Lattice strain measurement (*slow scan along x-axis*). (a)** Atomic resolution image of the nanoparticle, with the fast and slow scan axes shown. The refined atom positions overlaid on Figure S1(a) as blue dots. **(b) - (e)** ϵ_{xx}, ϵ_{xy}, ϵ_{θ} and ϵ_{yy} strain measured from the refined atom positions, with the graphically illustrated strain conventions shown in the bottom left of each individual strain map.

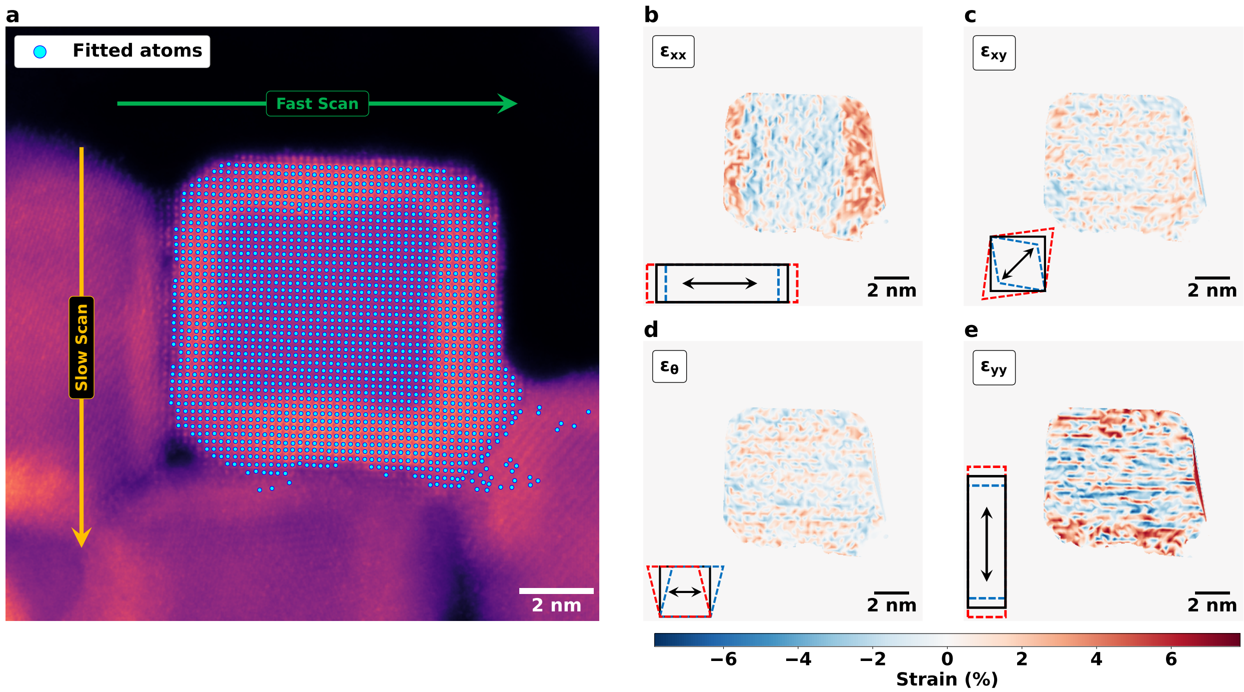

Figure S2: **Lattice strain measurement (*slow scan along y-axis*).** **(a)** Atomic resolution image of the nanoparticle, with the fast scan and slow scan axes shown. The refined atom positions overlaid on Figure S2(a) as blue dots. **(b) - (e)** ϵ_{xx}, ϵ_{xy}, ϵ_{θ} and ϵ_{yy} strain measured from the refined atom positions, with the graphically illustrated strain conventions shown in the bottom left of each individual strain map.

This can lead to artifacts from scan distortions, as visible for example in Figure S1(b) as stripes and striations in the ϵ_{xx} strain maps. Similar confounding stripes can be observed in Figure S2(e) for the ϵ_{yy} strain maps. Notably the stripes ϵ_{xx} stripes in Figure S1(b) are absent in Figure S2(b) and vice-versa for the ϵ_{yy} features. This indicates that rather than being strain features in the material, they arise due to scan distortions, with the stripes originating perpendicular to the slow scan directions. In order to account for such distortions, these two orthogonal scan pairs were subsequently corrected for scanning distortions using MATLAB scripts developed originally by Ophus et. al.[S1]

2 Preconditioning diffraction data

Our two step data preconditioning routine proceeds as following:

1. **Logarithm of diffraction pattern:** The raw diffraction pattern is flattened in intensity space by taking the logarithm of the diffraction pattern. This is because for strain mapping, we are not interested in the features inside a diffraction disk, but rather the location of the disk itself, so taking the logarithm of the data smooths out the intensity variations of the diffraction disks themselves, and decreases the intensity variations between disks. Thus, if C is the CBED pattern, after the first step of preconditioning we obtain LC as shown in Equation 1

$$LC = log_{10}\left(1 + \frac{C - C_{min}}{C_{max} - C_{min}}\right) \tag{1}$$

   As could be ascertained from Equation 1, the pattern is normalized, so that the intensity values range from +1 to +2 to prevent taking logarithms of negative data, or values below 1.

2. **Sobel-Filtering:** We subsequently Sobel filter the logarithm of the CBED pattern (LC). The Sobel operators are two 3×3 kernels used frequently for edge detection

in computer vision.[S2,S3] When the kernels are convolved with an image, they give the approximate derivatives of the image along the two Cartesian directions of the image. The results from convolution with the two Sobel kernels – SC_x and SC_y are given as per Equation 2 and Equation 3 respectively, where LC is obtained as shown in Equation 1. $\otimes$ refers to convolution with a kernel.

$$SC_x = \begin{bmatrix} -1 & 0 & 1 \\ -2 & 0 & 2 \\ -1 & 0 & 1 \end{bmatrix} \otimes LC \tag{2}$$

$$SC_y = \begin{bmatrix} -1 & -2 & 1 \\ 0 & 0 & 0 \\ 1 & 2 & 1 \end{bmatrix} \otimes LC \tag{3}$$

Subsequently, we calculate the absolute magnitude of the Sobel derivative as per Equation 4

$$SC = \sqrt{SC_x^2 + SC_y^2} \tag{4}$$

If the first preconditioning step (Equation 1) is not followed, then Sobel filtering will pick up disk features as intensity variations, and along with *real* disk edges internal features will be highlighted too. The advantage of this two-step routine is that it is computationally relatively inexpensive to implement, but allows high-precision disk location without the need for specialized patterned condenser apertures.

The effects of preconditioning can be visualized in Figure S3, where the cross-correaltion peaks are significantly blurry for the raw datasets, sharper for logarithm of the CBED datasets and even sharper for preconditioned datasets. Additionally, as we can observe from Figure S3, preconditioning the pattern also allows for a larger number of diffraction disks to be fitted, and thus increasing the accuracy of unit cell quantification.

Similar to approaches adopted by Zeltzmann *et. al.*,[S4] we followed the cross-validation

(CV) approach for measuring the error of peak fitting. In this procedure the disk fitting and strain measurement is performed twice. For every dataset,apart from the central $\langle 000 \rangle$, half the disks are fitted, while in the second measurement the $\langle 000 \rangle$ disk and the other disks that were not fitted the first time are fitted. The calculated unit cell is compared between the two measurements - which is the CV error.

We observed a CV error of raw data at **0.216%**, for logarithm of the CBED data at **0.1962%** and an error of **0.074%** for preconditioned data. The preconditioned data is thus approximately 3 times more accurate than the raw data, and demonstrates performance similar to bulls-eye apertures.[S4]

3 Region identification with MCR

Due to *Z contrast* in atomic resolution HAADF-STEM, distinction can be made between the core and shell of the nanoparticle through atom column intensities too, as demonstrated in Figure S4. However, the intensity of each individual atom columns depends not only on the atomic (Z) number, but also the total number of atoms in that column. As a result, as could be observed in Figure S4, a simple partitioning of the intensities into two sets – below and above the median intensity of the columns is close but not completely accurate.

Going by this simplistic scheme, the edges of the nanocube which have lesser number of atoms in each column will be erroneously assigned to the particle core rather than the shell. However, a nanoparticle is a special case, and in many other examples like thin films the sample thickness is pretty uniform and intensity distributions can be used for region identification from ADF-STEM datasets.

In 4D-STEM nanodiffraction however individual atom columns are not distinguishable so a region identification scheme would need to distinguish based on the diffraction patterns at individual scan positions itself.

MCR requires template spectra for matching. The spectra in this case was chosen

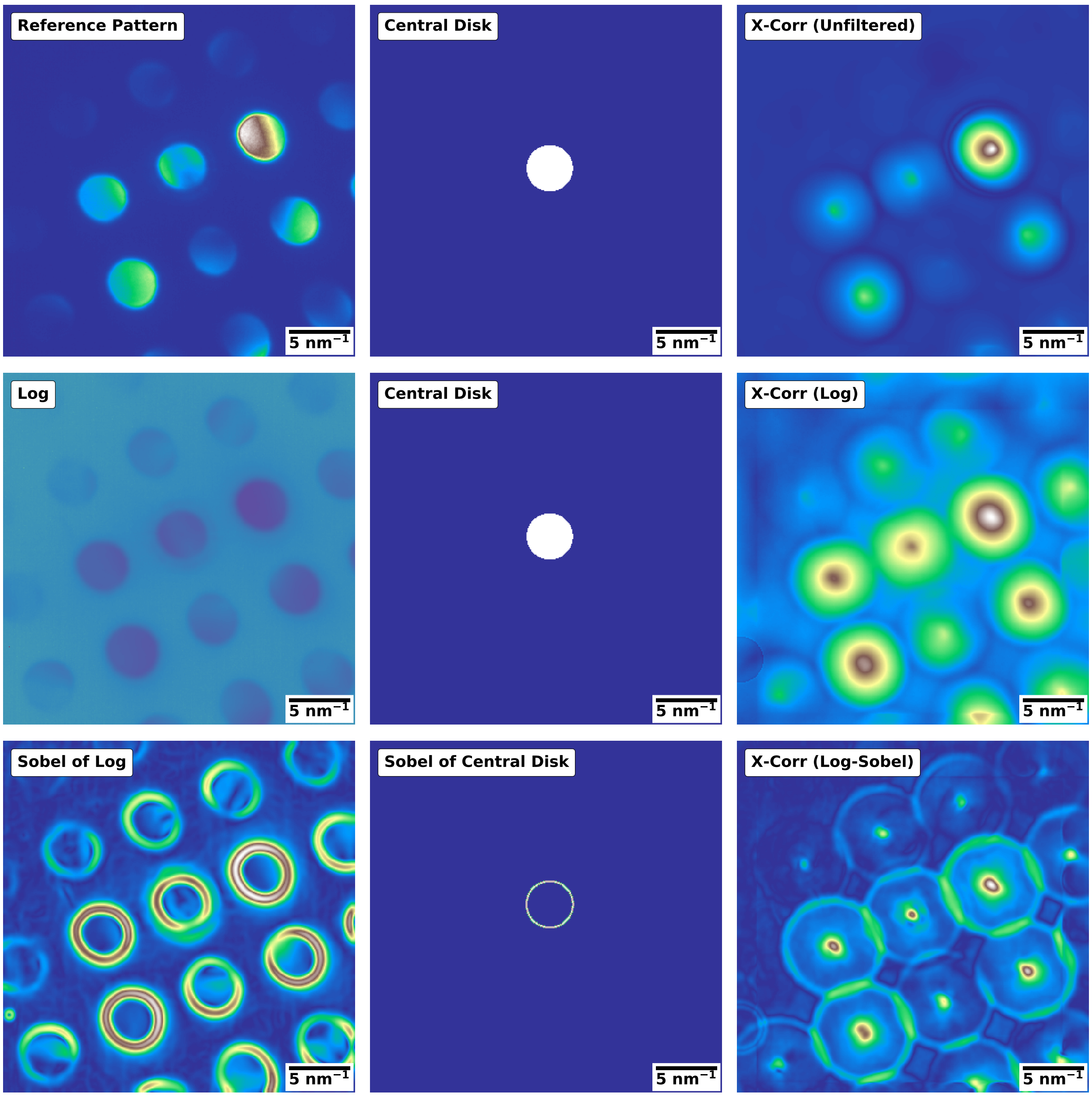

Figure S3: **Effect of preconditioning on peak sharpness**

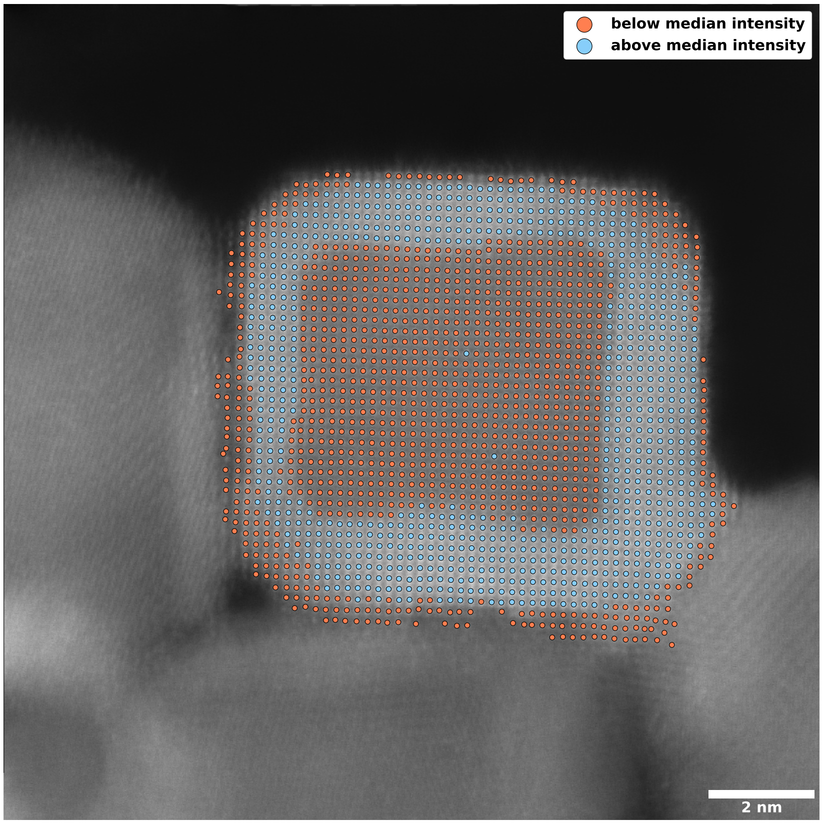

Figure S4: **Intensity distribution of atom columns in ADF-STEM**

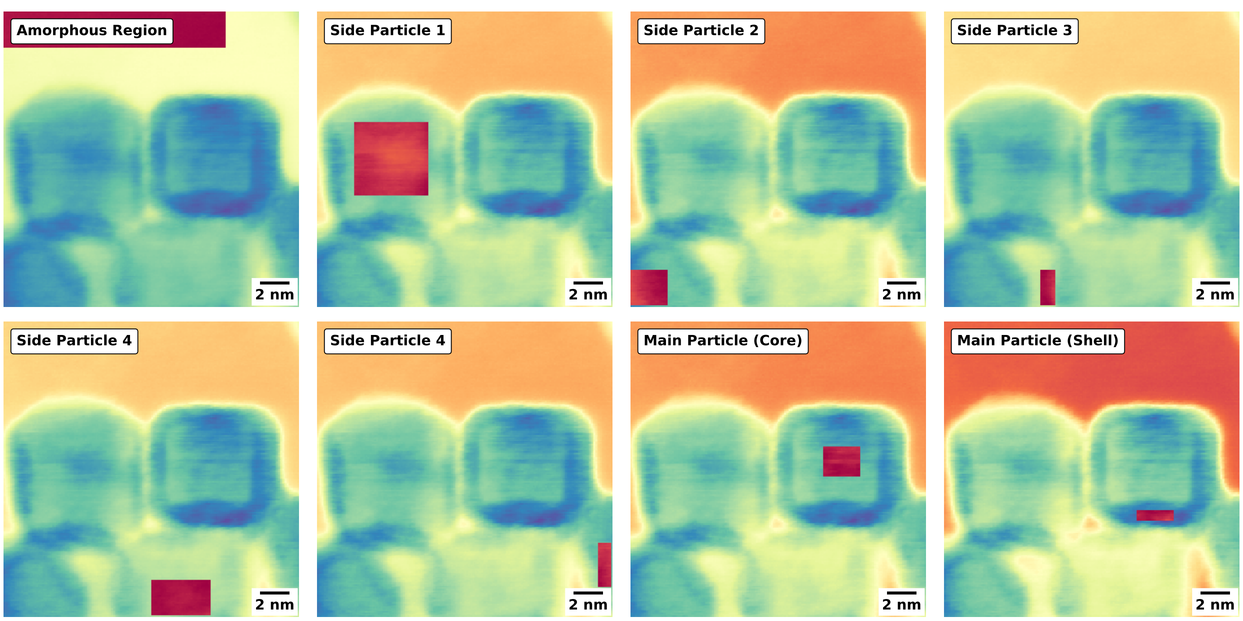

Figure S5: **Regions of Interest (ROI) chosen manually for location identification with MCR, overlaid as red rectangles on the images** manually, by selecting a region of the sample, with the mean CBED pattern from that region being the template spectra. The regions are demonstrated in Figure S5, with each neighboring particle, the amorphous region and the particle core and the particle shell being chosen as templates.

Since MCR can only match 1D spectra, the CBED patterns from each region are first downsampled by a factor of 4, and then unrolled as a 1D spectra. This is then compared with the unrolled, downsampled CBED spectra from every scanning point for region identification.

MCR was performed on the unprocessed data (Figure S6), the logarithm of the data (Figure S7) and the preconditioned data (Figure S8). Similar to the advantages of data preconditioning for strain mapping, we observed MCR actually performed better on logarithm of CBED patterns rather than the raw patterns, with preconditioned data outperforming both of them for region identification.

References

(S1) Ophus, C.; Ciston, J.; Nelson, C. T. Correcting nonlinear drift distortion of scanning probe and scanning transmission electron microscopies from image pairs with orthogonal scan directions. *Ultramicroscopy* **2016**, *162*, 1–9.

(S2) Sobel, I.; Feldman, G. A 3×3 isotropic gradient operator for image processing. *A Talk at the Stanford Artificial Project* **1968**, 271–272.

(S3) Kanopoulos, N.; Vasanthavada, N.; Baker, R. L. Design of an image edge detection filter using the Sobel operator. *IEEE J. Solid-State Circuits* **1988**, *23*, 358–367.

(S4) Zeltmann, S. E.; Müller, A.; Bustillo, K. C.; Savitzky, B.; Hughes, L.; Minor, A. M.; Ophus, C. Patterned Probes for High Precision 4D-STEM Bragg Measurements. *Ultramicroscopy* **2020**, *209*, 112890.

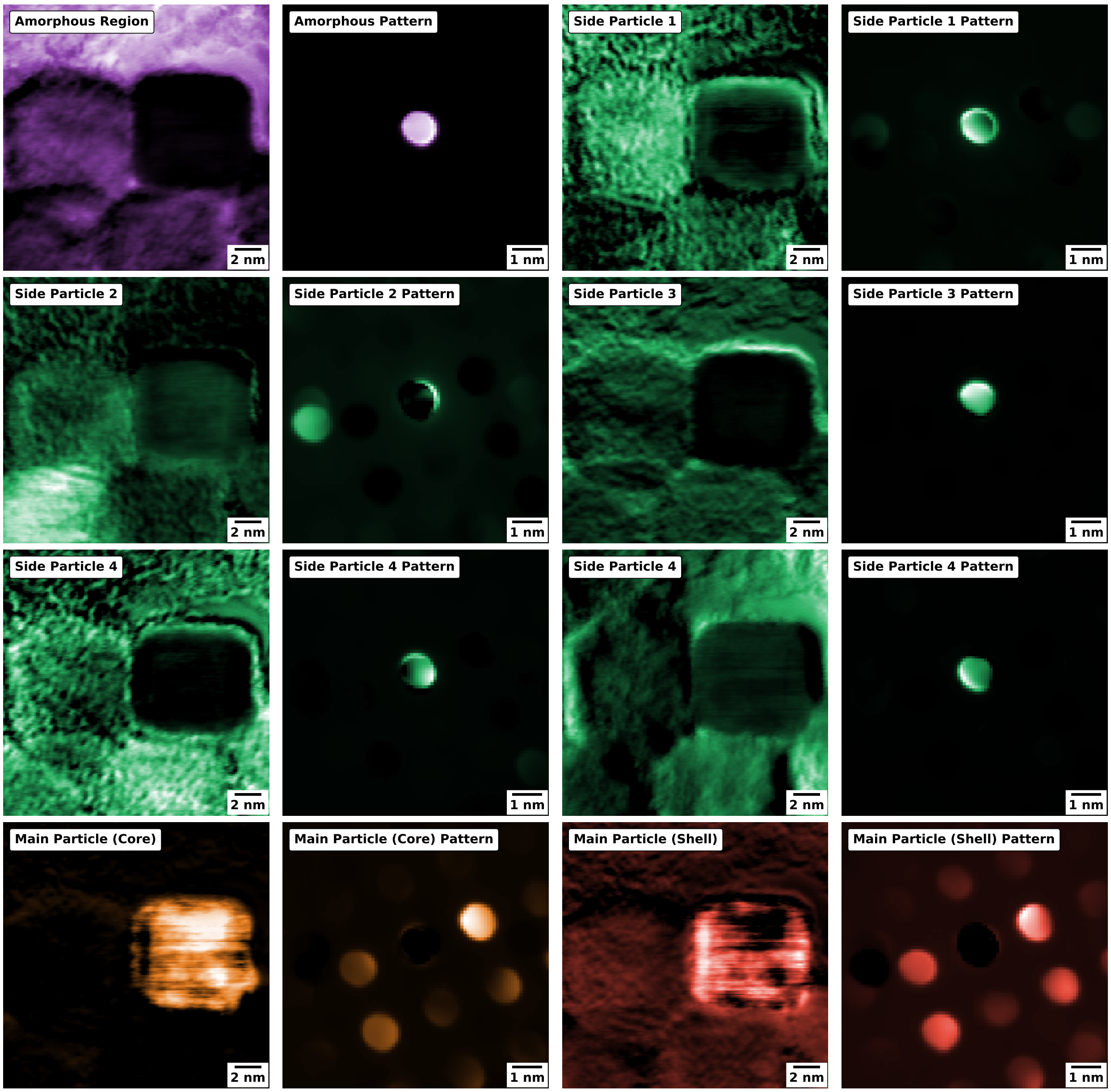

Figure S6: **MCR Results on unfiltered CBED patterns**

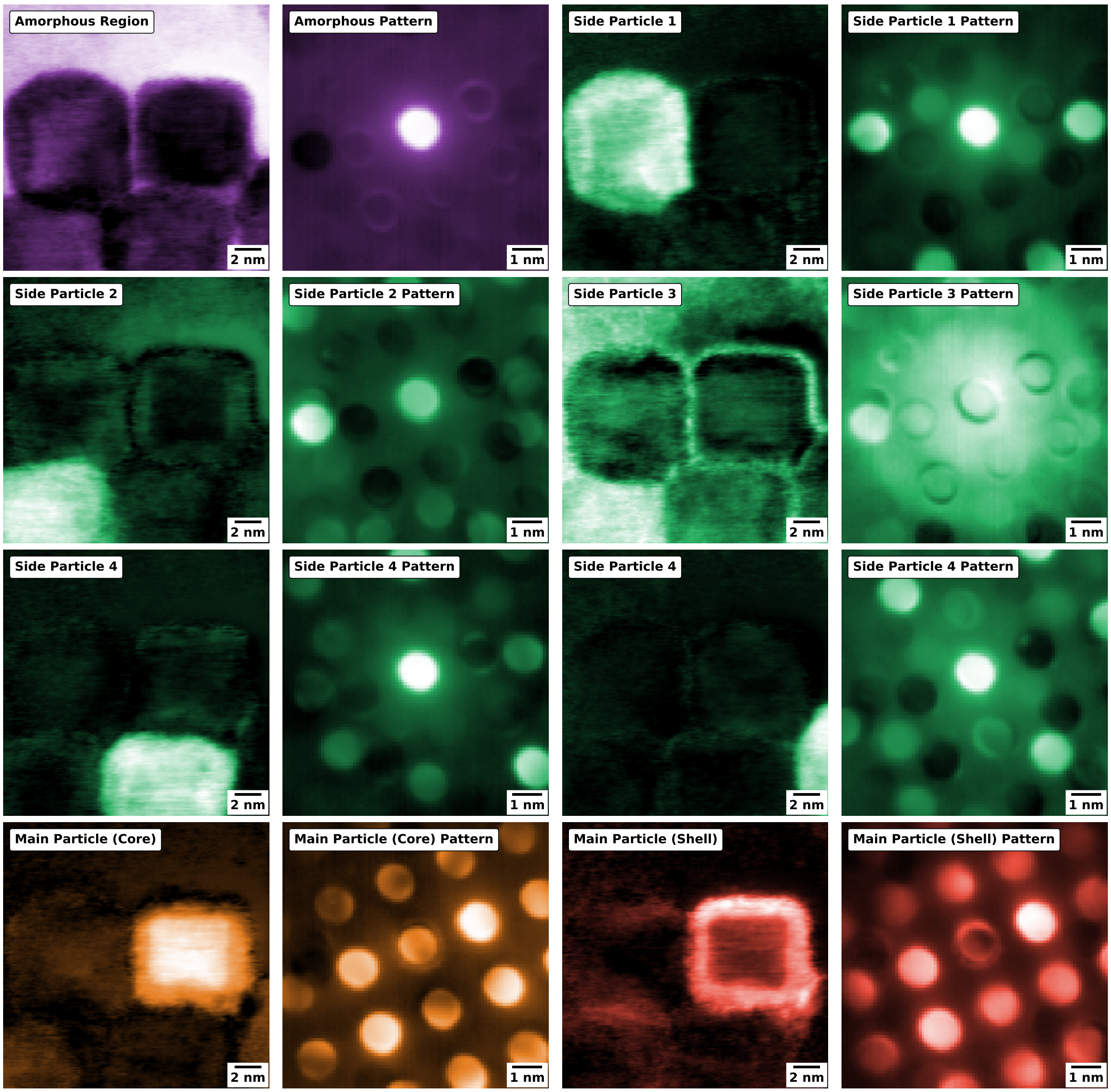

Figure S7: **MCR Results on log of CBED patterns**

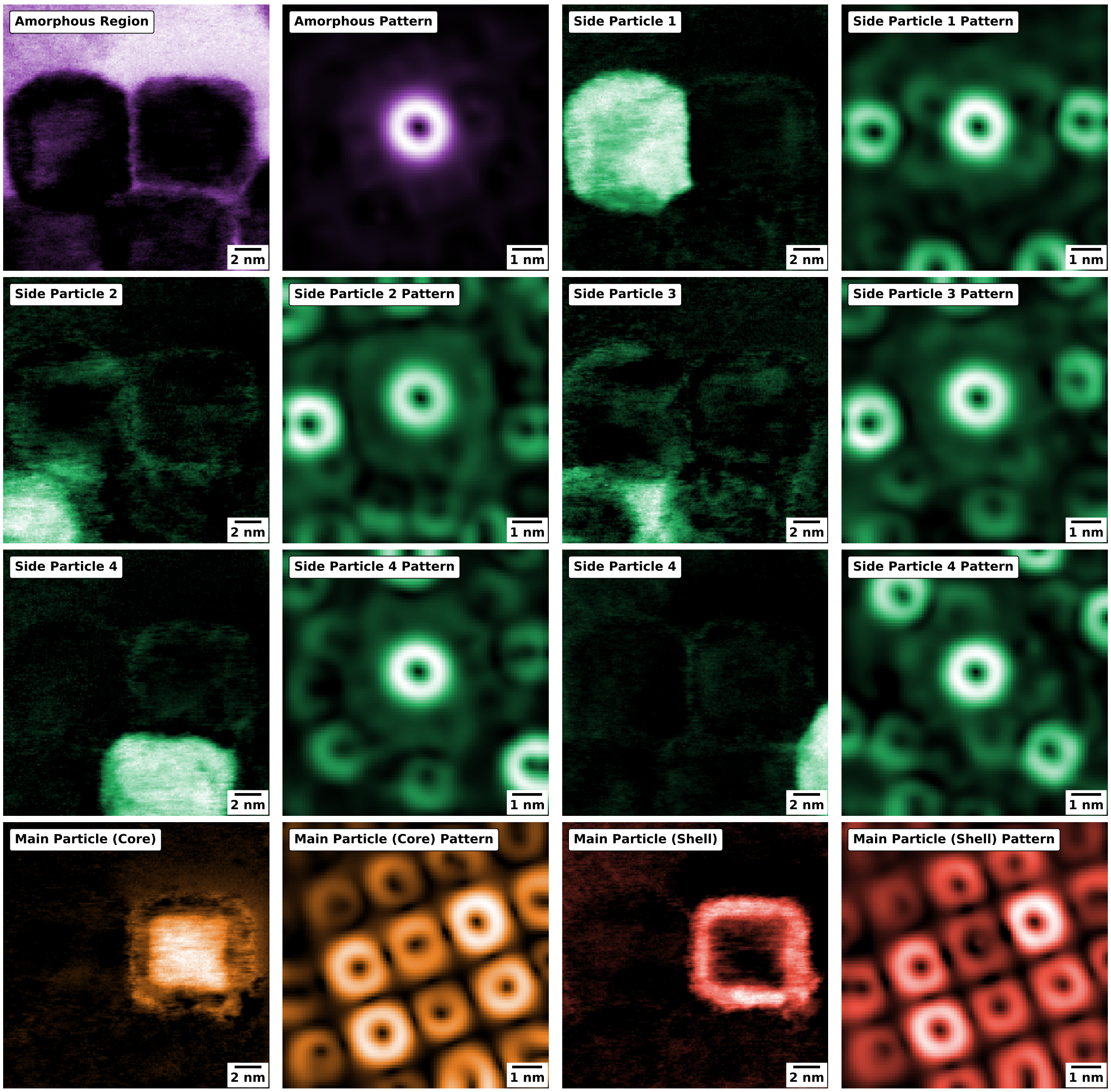

Figure S8: **MCR Results on Preconditioned CBED patterns**